THEORETICAL AND APPLIED MECHANICS
Volume 48 (2021) Issue 1, 39–51 DOI: https://doi.org/10.2298/TAM200402010K

STABILITY OF PINNED–ROTATIONALLY RESTRAINED ARCHES

László Péter Kiss

Abstract. The article aims to find the buckling loads for pinned–rotationally restrained shallow circular arches in terms of the rotational end stiffness, geometry and material distribution. The loading is a concentrated vertical force placed at the crown. A geometrically nonlinear model is presented which relates not only the axial force but also the bending moment to the membrane strain. The nonlinear load-strain relationship is established between the strain and load parameters. This equation is then solved and evaluated analytically. It turns out that the stiffness of the end-restraint has, in general, a significant effect on the lowest buckling load. At the same time, some geometries are not affected by this. As the stiffness becomes zero, the arch is pinned-pinned and as the stiffness tends to infinity, the arch behaves as if it were pinned-fixed and has the best load-bearing abilities.

1. Introduction

Although the buckling of straight columns has long been known, such members are still under extensive investigations with relevant new findings [1, 11, 16–19]. At the same time, various other structural elements, like slender arches, must also be checked for buckling to prevent unexpected failure. Within this topic, there are books available containing the basics and more [4, 6, 24]. Furthermore, paper [15] analytically focuses on the static stability of pinned arches by means of a variational principle. The model in [30] assumes imperfect shallow arches and presents solutions for remote, unconnected equilibrium branches. Article [10] is devoted to elastically supported steel arches. Both simulations and experiments are described and compared. An integral equation procedure is described and solved with the analog equation method in [28] for arches with a geometrically non-uniform cross-section. The stability of three-pinned arches is tackled analytically in [22] with linear and nonlinear models being compared. In [23] a novel numerical method is developed for the nonlinear stability analysis of various curved elements. The model also accounts for the foundation position and stiffness. The behavior of

2010 *Mathematics Subject Classification:* 74G60; 74B15.
Key words and phrases: arch, buckling, stiffness, snap-through.

various nonhomogeneous structural elements is also the subject of ongoing research [2, 3, 7–9, 29].

Moreover, articles [5, 12, 20, 21, 25–27] should also be mentioned. These works commonly use the Euler–Bernoulli hypothesis with geometrical nonlinearities incorporated to find out the circumstances, conditions and characteristics for the buckling of shallow arches under diverse conditions. These include various support and load conditions, uniform and varying cross-section geometries, and also the material distribution is nonhomogeneous in some cases.

This article aims to investigate the planar stability of pinned–rotationally restrained shallow arches. The elastic support is modeled by a linear torsional spring. As for the kinematics, the one-dimensional model uses the Euler-Bernoulli hypothesis. The strains are small and the rigid body rotations are moderately large. The geometrically nonlinear model incorporates nonhomogeneous material distributions along the thickness of the arch. Static equilibrium equations are derived and solved in closed-form. The effect of the spring stiffness and, geometrical-material distribution on the (critical) buckling load is investigated. As the spring stiffness is set to zero, the arch becomes pinned-pinned, and as the stiffness tends to infinity, the arch behaves as if it were pinned-fixed.

2. Basic equations

The considered one-dimensional arch with included angle $\theta = 2\vartheta$, radius ρ_o is supported by an ideal pin at the left end and by a rotationally restrained pin with spring constant k_γ at the right end. The E-weighted centerline with the supports and radial dead load P_ζ are shown in Figure 1. The local base is also shown in this figure with axis η being the principal axis of the cross-section, $\xi = s$ noting the tangential direction and ζ, furthermore, lies in the plane of the centerline. Derivations taken with respect to the arc coordinate s and the angle coordinate φ are noted in short throughout the article by

$$\frac{\mathrm{d}^n(\ldots)}{\mathrm{d}s^n} = \frac{1}{\rho_o^n}\frac{\mathrm{d}^n(\ldots)}{\mathrm{d}\varphi^n} = (\ldots)^{(n)}, \quad n \in \mathbb{Z}.$$

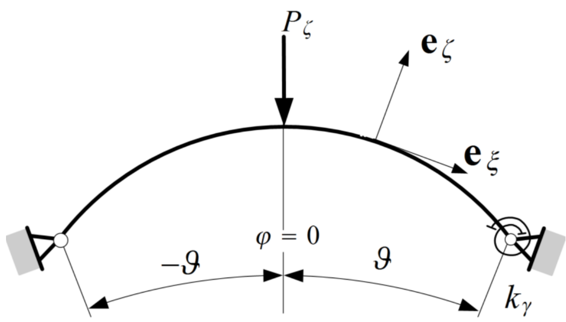

FIGURE 1. The one-dimensional arch model

With the classical Euler-Bernoulli hypothesis [13], the axial strain at an arbitrary point and that on the centerline are assumed to be

$$\varepsilon_\xi = \frac{\rho_o}{\rho_o+\zeta}(\varepsilon_{o\xi}+\zeta\kappa_o)+0.5\psi_{o\eta}; \quad \varepsilon_m = \varepsilon_\xi|_{\zeta=0} = \varepsilon_{o\xi}+0.5\psi^2_{o\eta} \tag{2.1}$$

with

$$\varepsilon_{o\xi} = \frac{\mathrm{d}u_o}{\mathrm{d}s}+\frac{w_o}{\rho_o}, \quad \psi_{o\eta} = \frac{u_o}{\rho_o}-\frac{\mathrm{d}w_o}{\mathrm{d}s}.$$

The latter is the cross-sectional rigid body rotation and its first derivative is the κ_o curvature. The membrane strain is nonlinear through the infinitesimal rotations.

Possibly, there is cross-sectional inhomogeneity, meaning that the material parameters – like the elasticity modulus E – can be the function of the η,ζ coordinates: $E(\eta,\zeta) = E(-\eta,\zeta)$. As the material is linearly elastic, isotropic the constitutive equation yields

$$N = \int_A E\varepsilon_\xi \mathrm{d}A \approx A_e\varepsilon_m - \frac{I_{e\eta}}{\rho_o}\kappa_o, \tag{2.2}$$

$$M = \int_A E\varepsilon_\xi\zeta\,\mathrm{d}A = -I_{e\eta}\Big(\frac{\mathrm{d}^2 w_o}{\mathrm{d}s^2}+\frac{w_o}{\rho_o^2}\Big) \tag{2.3}$$

for the axial force and the bending moment. Here,

$$A_e = \int_A E(\eta,\zeta) \quad I_{e\eta} = \int_A \zeta^2 E(\eta,\zeta)\mathrm{d}A \tag{2.4}$$

are called the E-weighted area and moment of inertia.

From now on, an * symbol denotes that a quantity is considered in the post-buckling equilibrium and $_b$ is the increment, i.e., the change between the pre- and post-buckling states. With this decomposition, the following relations hold for the various kinematical quantities [12]:

$$\psi^*_{o\eta} = \psi_{o\eta}+\psi_{o\eta b}, \quad \psi_{o\eta b} = \frac{u_{ob}}{\rho_o}-\frac{\mathrm{d}w_{ob}}{\mathrm{d}s}, \quad \varepsilon_{o\xi b} = \frac{\mathrm{d}u_{ob}}{\mathrm{d}s}+\frac{w_{ob}}{\rho_o}\ ,$$

$$\varepsilon_{\xi b} = \frac{\rho_o}{\rho_o+\zeta}(\varepsilon_{o\xi b}+\zeta\kappa_{ob})+\psi_{o\eta}\psi_{o\eta b}; \quad \varepsilon_{mb} = \varepsilon_{o\xi b}+\psi_{o\eta b}\psi_{o\eta}. \tag{2.5}$$

With (2.2), (2.3), (2.4), and (2.5) the total and incremental parts of the axial force and bending moment are

$$N^* = \int_A E\varepsilon^*_\xi \mathrm{d}A = N+N_b, \qquad N_b = A_e\varepsilon_{mb}-\frac{I_{e\eta}}{\rho_o}\kappa_{ob},$$

$$M^* = \int_A E\varepsilon^*_\xi\zeta\,\mathrm{d}A = M+M_b, \qquad M_b = -I_{e\eta}\Big(\frac{\mathrm{d}^2 w_{ob}}{\mathrm{d}s^2}+\frac{w_{ob}}{\rho_o^2}\Big).$$

We introduce notations

$$A_e\rho_o^2/I_{e\eta} = (\rho_o/r)^2 = m, \quad r = \sqrt{I_{e\eta}/A_e}\ ,$$

which are referred to as the E-weighted radius of gyration r and the modified slenderness ratio of the arch m.

3. Pre- and post-buckling equilibrium

Similarly to [14], from the principle of virtual work for the pre-buckling static equilibrium, the following equations must be satisfied

$$\begin{aligned} &\frac{\mathrm{d}N}{\mathrm{d}s} + \frac{1}{\rho_o}\Big[\frac{\mathrm{d}M}{\mathrm{d}s} - \Big(N + \frac{M}{\rho_o}\Big)\psi_{o\eta}\Big] = 0, \\ &\frac{\mathrm{d}}{\mathrm{d}s}\Big[\frac{\mathrm{d}M}{\mathrm{d}s} - \Big(N + \frac{M}{\rho_o}\Big)\psi_{o\eta}\Big] - \frac{N}{\rho_o} = 0, \end{aligned} \tag{3.1}$$

while the associated boundary conditions for a pinned–rotationally restrained arch are

$$w_o|_{\pm\vartheta} = M|_{-\vartheta} = (M + k_\gamma \psi_{o\eta})|_\vartheta = 0.$$

Furthermore, the discontinuity condition

$$\Big[\frac{\mathrm{d}M}{\mathrm{d}s} - \Big(N + \frac{M}{\rho_o}\Big)\psi_{o\eta}\Big]_{+0} - \Big[\frac{\mathrm{d}M}{\mathrm{d}s} - \Big(N + \frac{M}{\rho_o}\Big)\psi_{o\eta}\Big]_{-0} - P_\zeta = 0$$

must also be satisfied.

Equilibrium equations (3.1) with the use of Equations (2.1)–(2.4) can be given [12] by

$$\frac{\mathrm{d}}{\mathrm{d}s}(A_e\varepsilon_m) = 0 \quad \rightarrow \quad \varepsilon_m = \text{constant} \tag{3.2}$$

and

$$W_o^{(4)} + (\chi^2 + 1)W_o^{(2)} + \chi^2 W_o = \chi^2 - 1, \quad \chi^2 = 1 - m\varepsilon_m, \tag{3.3}$$

with the dimensionless radial displacement $W_o = w_o/\rho_o$. It is, therefore, found that the membrane strain is constant under the action of a central concentrated load. As for (3.3), the general solution is

$$W_o(\varphi) = \frac{\chi^2 - 1}{\chi^2} + A_1\cos\varphi + A_2\sin\varphi - \frac{A_3}{\chi^2}\cos\chi\varphi - \frac{A_4}{\chi^2}\sin\chi\varphi$$

in the range $\varphi \in [-\vartheta; 0]$ and is

$$W_o(\varphi) = \frac{\chi^2 - 1}{\chi^2} + B_1\cos\varphi + B_2\sin\varphi - \frac{B_3}{\chi^2}\cos\chi\varphi - \frac{B_4}{\chi^2}\sin\chi\varphi$$

in $\varphi \in [0; \vartheta]$. The former constants $A_i; B_i$ can be given using the boundary, continuity and discontinuity conditions, which yield a homogeneous system of linear equations for the unknowns:

$$\begin{bmatrix} \cos\vartheta & -\sin\vartheta & -\frac{\cos\chi\vartheta}{\chi^2} & \frac{\sin\chi\vartheta}{\chi^2} & 0 & 0 & 0 & 0 & 0 \\ -\chi\sin\vartheta & -\chi\cos\vartheta & \sin\chi\vartheta & \cos\chi\vartheta & 0 & 0 & 0 & 0 & 0 \\ 1 & 0 & -\frac{1}{\chi^2} & 0 & -1 & -1 & 0 & \frac{1}{\chi^2} & 0 \\ 0 & -\chi & 0 & 1 & 0 & 0 & \chi & 0 & -1 \\ -1 & 0 & 1 & 0 & 1 & 1 & 0 & -1 & 0 \\ 0 & 1 & 0 & -\chi & 0 & 0 & -1 & 0 & \chi \\ 0 & 0 & 0 & 0 & \cos\vartheta & \cos\vartheta & \sin\vartheta & -\frac{\cos\chi\vartheta}{\chi^2} & -\frac{\sin\chi\vartheta}{\chi^2} \\ 0 & 0 & 0 & 0 & \mathcal{S}\chi\sin\vartheta-\cos\vartheta & \mathcal{S}\chi\sin\vartheta-\cos\vartheta & -\mathcal{S}\chi\cos\vartheta-\sin\vartheta & \cos\chi\vartheta-\mathcal{S}\sin\chi\vartheta & \mathcal{S}\cos\chi\vartheta+\sin\chi\vartheta \end{bmatrix} \times \begin{bmatrix} A_1 \\ A_2 \\ A_3 \\ A_4 \\ B_1 \\ B_2 \\ B_3 \\ B_4 \end{bmatrix} = \begin{bmatrix} -\frac{\chi^2-1}{\chi^2} \\ 0 \\ 0 \\ 0 \\ 0 \\ \frac{-2\mathcal{P}}{\vartheta} \\ -\frac{\chi^2-1}{\chi^2} \\ 0 \end{bmatrix}. \tag{3.4}$$

The new notations $\mathcal{S} = \rho_o k_\gamma / I_{e\eta}$ and $\mathcal{P} = -P_\zeta \rho_o^2 \vartheta / 2I_{e\eta}$ are for the dimensionless spring stiffness and the dimensionless load. Clearly, if $\mathcal{S} = 0$ / $\mathcal{S} \to \infty$ the results are the same as for a pinned-pinned / pinned-fixed arch [13].

Recalling now equilibrium equation (3.2), because the membrane strain is constant, the mathematical average of the strain, i.e., the strain itself, is given by

$$\varepsilon_m = \frac{1}{2\vartheta}\int_{-\vartheta}^{\vartheta} \varepsilon_m \mathrm{d}\varphi = \frac{1}{2\vartheta}\int_{-\vartheta}^{\vartheta} \Big(\varepsilon_{o\xi} + \frac{1}{2}\psi_{o\eta}^2\Big)\mathrm{d}\varphi.$$

After carrying out these integrations, the resultant is a quadratic formula, which is the nonlinear connection between the load and strain

$$C_2\mathcal{P}^2 + C_1\mathcal{P} + C_0 = 0, \quad C_j(m,\vartheta,\chi,\mathcal{S}) \in \mathbb{R}, \qquad j = 0,1,2 \tag{3.5}$$

and it must hold for any parameter set.

The principle of virtual work for the buckled configuration yields [14] coupled differential equations

$$\begin{gathered} \frac{\mathrm{d}N_b}{\mathrm{d}s} + \frac{1}{\rho_o}\frac{\mathrm{d}M_b}{\mathrm{d}s} - \frac{1}{\rho_o}\Big(N + \frac{M}{\rho_o}\Big)\psi_{o\eta b} - \frac{1}{\rho_o}\Big(N_b + \frac{M_b}{\rho_o}\Big)\psi_{o\eta b} = 0, \\ \frac{\mathrm{d}^2 M_b}{\mathrm{d}s^2} - \frac{N_b}{\rho_o} - \frac{\mathrm{d}}{\mathrm{d}s}\Big[\Big(N + N_b + \frac{M+M_b}{\rho_o}\Big)\psi_{o\eta b} + \Big(N_b + \frac{M_b}{\rho_o}\Big)\psi_{o\eta}\Big] = 0. \end{gathered} \tag{3.6}$$

The boundary conditions are

$$w_{ob}|_{\pm\vartheta} = M_b|_{-\vartheta} = (M_b + k_\gamma \psi_{o\eta b})|_{\vartheta} = 0.$$

Moreover, as there is no increment in the load, all the typical fields are continuous throughout the arch. Equations (3.6) can be manipulated [14] so that

$$\frac{\mathrm{d}}{\mathrm{d}s}(A_e \varepsilon_{mb}) = 0 \quad \to \quad \varepsilon_{mb} = \text{constant} \tag{3.7}$$

and

$$W_{ob}^{(4)} + (\chi^2 + 1)W_{ob}^{(2)} + \chi^2 W_{ob} = m\varepsilon_{mb}[1 - (W_o^{(2)} + W_o)]. \tag{3.8}$$

The solution to (3.8) assumes

$$W_{ob}(\varphi) = D_1 \cos\varphi + D_2 \sin\varphi + D_3 \sin\chi\varphi + D_4 \cos\chi\varphi \\ - \frac{m\varepsilon_{mb}}{2\chi^3}\Big(\frac{2}{\chi} + X_3\varphi \sin\chi\varphi - X_4 \varphi\cos\chi\varphi\Big),$$

with X_i being A_i if $\varphi \in [-\vartheta; 0]$ and B_i if $\varphi \in [0; \vartheta]$ – these are known from (3.4). The new coefficients D_j can be expressed in closed-form from the boundary and continuity conditions.

With the strain increment being constant, equilibrium equation (3.7) yields another quadratic relation between the dimensionless load $\mathcal{P}$ and the strain parameter χ:

$$\varepsilon_{mb} = \frac{1}{2\vartheta}\int_{-\vartheta}^{\vartheta} (\varepsilon_{mb} + \psi_{o\eta}\psi_{o\eta b})\mathrm{d}\varphi = F_2\mathcal{P}^2 + F_1\mathcal{P} + F_0. \tag{3.9}$$

Solving Eqs. (3.5)–(3.9) simultaneously for the two unknowns $\mathcal{P}, \chi$ makes it possible to tackle the stability issue.

It must be noted that, in a special case, when $\mathcal{S} = 0$ (the arch is pinned-pinned) and the pre-buckling deformations are symmetric to axis $\zeta(\varphi = 0)$, it is possible for bifurcation buckling to occur. It means that with zero strain increment, the arch buckles to an infinitesimally close equilibrium configuration [5]. Hence, equation (3.8) becomes homogeneous and since it is paired with homogeneous boundary conditions, the following characteristic equation can be established:

$$(1-\chi)^2(1+\chi)^2 \sin\chi\vartheta \cos\chi\vartheta \cos\vartheta \sin\vartheta = 0.$$

The lowest true solution for the strain (actually, the critical strain for bifurcation buckling) follows from the term $\sin\chi\vartheta$ and is

$$\varepsilon_m = \frac{\vartheta^2 - \pi^2}{m\vartheta}. \tag{3.10}$$

Plugging (3.10) back to (3.5) makes it possible to evaluate the buckling loads for bifurcation buckling.

In relation to pinned-pinned arches, it is proven in [13] that for smaller central angles, limit point buckling can be expected as there is either no bifurcation point or it is on an unstable equilibrium branch. Then, increasing ϑ, the bifurcation point moves to the primary stable branch so that type of buckling occurs first (at a lower strain). As for pinned-fixed and pinned–rotationally restrained members, clearly, there is only limit point buckling.

4. Computational results

The detailed investigations are carried out in terms of various parameters like the dimensionless spring stiffness $\mathcal{S} \in [0; \infty]$, semi-vertex angle $\vartheta \in [0; 0.4\pi]$, quotient of the arch length and radius of gyration $S/r \in [75; 150]$. In the following figures, always the lowest buckling loads are plotted.

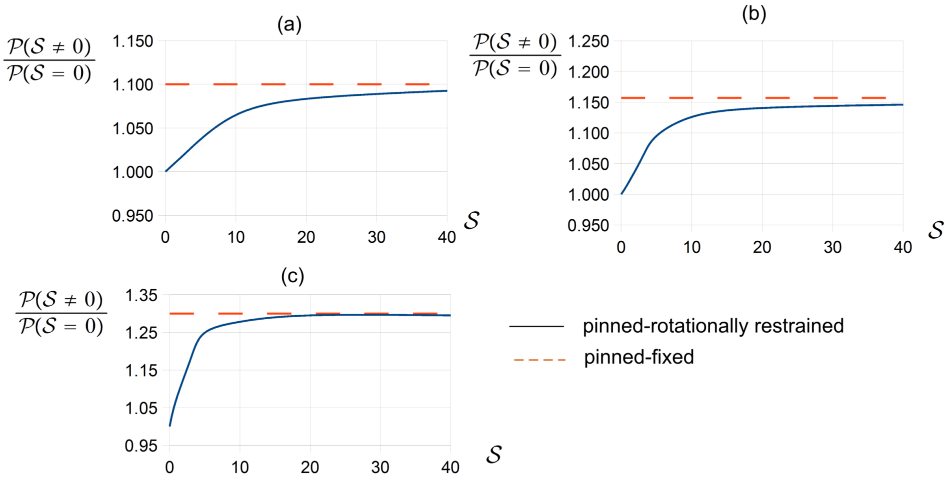

FIGURE 2. Variation of the critical load ratio in terms of the spring stiffness if (a) $\vartheta = 0.4$; (b) $\vartheta = 0.8$; (c) $\vartheta = 1.2$

It is first shown how the critical load ratio $\mathcal{P}(\mathcal{S} \neq 0)/\mathcal{P}(\mathcal{S} = 0)$ varies with $\mathcal{S}$ and ϑ. Three semi-vertex angles are selected this time: 0.4, 0.8 and 1.2. According to the computational results, the curves in Figure 2 are independent of S/r. The dashed lines represent the limit solution $(\mathcal{S} \to \infty)/(\mathcal{S} = 0)$. Moreover, as ϑ is increased, the load ratio visibly increases. Furthermore, convergence in $\mathcal{S}$ is quite quick – it can be said that, in this respect, arches with spring stiffness above 40 behave like pinned-fixed members. This finding is independent of both S/r and ϑ.

In Figures 3 and 5, four values of $\mathcal{S}$ are selected $(0; 2; 5; 10^{10})$ to show the effect of the stiffness of the rotational end restraint in terms of S/r and ϑ. In Figure 3, it is clear that the softest support condition is the pinned-pinned one with the related lowest buckling loads. However, in a small central angle range – $\vartheta \in [0.28; 0.32]$ – the buckling load is actually independent of the support stiffness. Otherwise, the effect of $\mathcal{S}$ is greatest when the angle is greatest. It is clear that the spring stiffness has considerable effects. Similar findings are valid for $S/r = \{100; 150\}$ in Figures 4 and 5. For the pinned-pinned case, the buckling loads tend to decrease after a while but for other supports, there is a monotonous increase. The curves shift to the left with S/r increased.

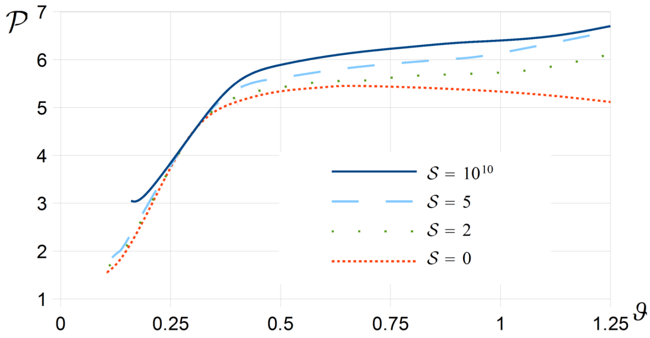

FIGURE 3. Critical loads for $S/r = 75$

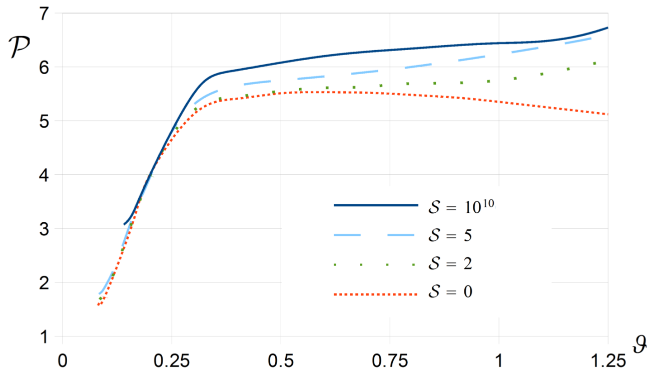

FIGURE 4. Critical loads for $S/r = 100$

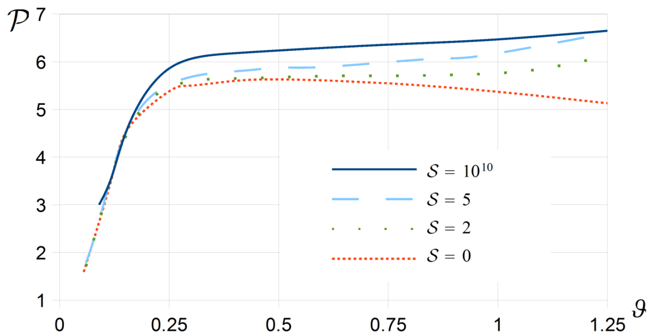

FIGURE 5. Critical loads for $S/r = 150$

Fixing the end-restraint stiffness to 5, Figure 6 shows how S/r affects the buckling loads. For smaller central angles, the buckling load increases together with S/r and the solutions are quite distinct. However, around $\vartheta \simeq 0.6$ the curves coincide with a good accuracy and tend to the same limit. Therefore, it can be concluded that starting from $\vartheta \geqslant 0.6$, the buckling load in independent of S/r.

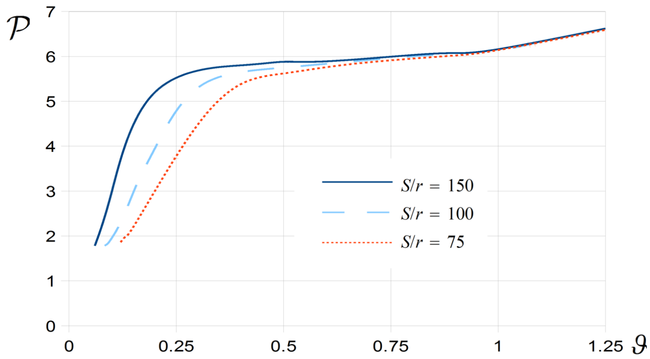

FIGURE 6. The effect of S/r when $\mathcal{S} = 5$

Finally, Figures 7 and 8 depict the in-plane static behavior of arches. The dimensionless load $\mathcal{P}$ is plotted against the strain ratio – this latter is the actual strain divided by the critical (buckling) strain for pinned-fixed members: $\varepsilon_m(\mathcal{S})/\varepsilon_m(\mathcal{S} = 10^{10})$. Two angles are selected ($\vartheta = 0.15; 0.3$) with S/r set to 100. In Figure 7, it is clearly visible that while the critical strain is lowest for the pinned-fixed case, it holds the greatest buckling load. One branch in all these curves starts from the origin, while the other branch starts from a different level – this latter value increases with $\mathcal{S}$. At the upper point where the tangent becomes zero, there is buckling.

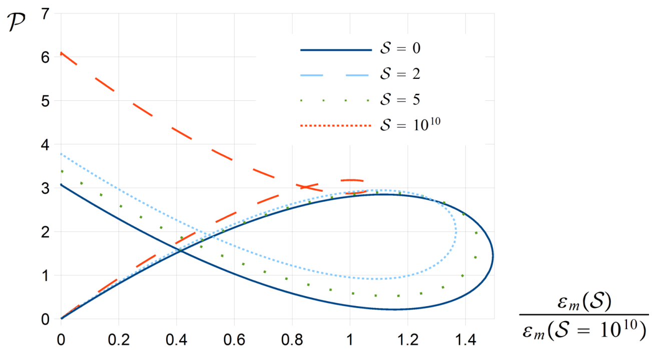

FIGURE 7. Load-strain relationships for $S/r = 100$ and $\vartheta = 0.15$

Meanwhile, in Figure 8 ($\vartheta = 0.3$), the behavior is much more complicated. For the pinned-fixed case, there is only one upper limit point (it holds the greatest buckling load), and for other spring stiffnesses, this number is two. Also, the buckling loads are quite close to each other – compare it with Figure 4. It turns out that for pinned-pinned supports only, the critical behavior is characterized by bifurcation buckling as this bifurcation point is closer to the origin as the limit point – see the marker.

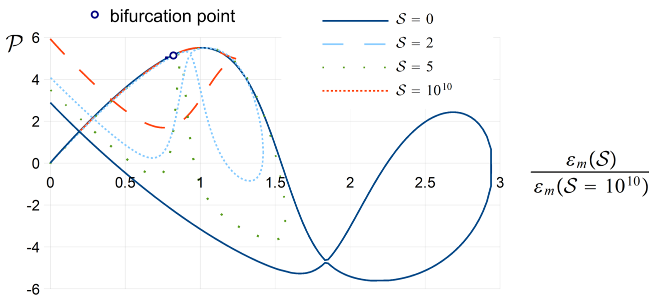

FIGURE 8. Load-strain relationships for $S/r = 100$ and $\vartheta = 0.3$

5. Conclusions

The in-plane stability of pinned–rotationally restrained shallow arches under a concentrated load was investigated. The rotational restraint was modeled by a linear torsional spring. The model is applicable if the material distribution is non-homogeneous and it changes along the cross-section. The classical Euler–Bernoulli hypothesis was used for the kinematical relations. The geometrically nonlinear model assumes infinitesimal strains and moderately large rotations. From the principle of virtual work, it was found that the membrane strain is constant not only in the pre-, but also in the post-buckling equilibrium state. The nonlinear relationships between the membrane strain parameter and the dimensionless load were given in closed form. It was found that when the spring stiffness is zero, the arch behaves as if it were pinned-pinned, while as this stiffness tends to infinity, the arch is actually pinned-fixed. The analytical results were evaluated in terms of various parameters, like the spring stiffness and geometry. The buckling loads were always the greatest for pinned-fixed and lowest for pinned-pinned arches. However, in a small range in the arch angle, the critical loads were actually independent of the spring stiffness.

Acknowledgments. The described article was carried out as part of the EFOP-3.6.1-16-2016-00011 "Younger and Renewing University – Innovative Knowledge City – institutional Development of the University of Miskolc Aiming at Intelligent Specialization" project implemented in the framework of the Szechenyi 2020 program. The realization of this project is supported by the European Union, co-financed by the European Social Fund and supported by the National Research, Development and Innovation Office - NKFIH, K115701.

References

1. M. A. Ali, M. Tomko, M. Badak, *Analysis of the resistance of thin-walled cold-formed compressed steel members with closed cross-sections. part* 1, Mag. Civ. Eng. **40**(5) (2013), 38–45.
2. R. J. Asaro, D. Benson, *Constitutive modeling for frp composite materials subject to extreme loading*, Theor. Appl. Mech. **45**(2) (2018), 205–230.
3. M. Bateni, M.R. Eslami, *Non-linear in-plane stability analysis of FGM circular shallow arches under central concentrated force*, Int. J. Non-Lin. Mech. **60** (2014), 58–69.
4. Z. Bazant, L. Cedolin, *Stability of Structures*, World Scientific, 2010.
5. M. A. Bradford, B. Uy, Y.-L. Pi, *In-plane elastic stability of arches under a central concentrated load*, J. Eng. Mech. **128**(2) (2002), 710–719.
6. C. L. Dym, *Stability Theory and its Applications to Structural Mechanics*, Dover, 1974, 2002.
7. E. E. Gdoutos, I. M. Daniel, *Failure modes of composite sandwich beams*, Theor. Appl. Mech. **35**(1–3) (2008), 105–118.
8. D. Gönczi, *Thermoelastic analysis of thick-walled functionally graded spherical pressure vessels with temperature-dependent material properties*, J. Comp. App. Mech. **12**(2) (2017), 109–125.
9. D. Gönczi, I. Ecsedi, *Thermoelastic stresses in nonhomogeneous prismatic bars*, Annals of Faculty of Engineering Hunedoara-Int. J. Eng. **13**(2) (2015), 49–52.
10. Q. Han, Y. Cheng, Y. Lu, T. Li, P. Lu, *Nonlinear buckling analysis of shallow arches with elastic horizontal supports*, Thin-Walled Struc. **109** (2016), 88–102.
11. C. C. Ike, C. U. Nwoji, B. O. Mama, H. N. Onah, M. E. Onyia, *Laplace transform method for the elastic buckling analysis of moderately thick beams*, Int. J. Eng. Res. Tech. **12**(10) (2019), 1626–1638.
12. L. Kiss, Gy. Szeidl, *In-plane stability of fixed-fixed heterogeneous curved beams under a concentrated radial load at the crown point*, Technische Mechanik **35**(1) (2015), 31–48.
13. L. Kiss, Gy. Szeidl, *Nonlinear in-plane stability of heterogeneous curved beams under a concentrated radial load at the crown point*, Technische Mechanik **35**(1) (2015), 1–30.
14. L. P. Kiss, *Nonlinear stability analysis of FGM shallow arches under an arbitrary concentrated radial force*, Int. J. Mech. Mat. Des. **16** (2020), 91–108.
15. V. Lalin, A. Dmitriev, S. Diakov, *Nonlinear deformation and stability of geometrically exact elastic arches*, Mag. Civ. Eng. **89**(5) (2019), 39–51.
16. K. Murawski, *Technical Stability of Continuously Loaded Thin-Walled Slender Columns*, Lulu Press, Inc., 2018.
17. K. Murawski, *Lateral Buckling in Elastic-Plastic States of Thin-Walled Semi-Slender Columns Made of Steel R35 According to Known Hypotheses*, (2020), pp. 47.
18. T. V. Nazmeeva, N. I. Vatin, *Numerical investigations of notched c-profile compressed members with initial imperfections*, Mag. Civ. Eng. **62**(2) (2016), 92–101.
19. O. Oguaghabmba, C. C. Ike, E. U. Ikwueze, I. Ofondu, *Finite fourier sine integral transform method for the elastic buckling analysis of doubly-symmetric thin-walled beams with dirichlet boundary conditions*, ARPN J. Eng. Appl. Sci. **14**(23) (2019), 3968–3974.
20. Y.-L. Pi, M. A. Bradford, *Non-linear buckling and postbuckling analysis of arches with unequal rotational end restraints under a central concentrated load*, Int. J. Sol. Struc. **49** (2012), 3762–3773.
21. Y.-L. Pi, M. A. Bradford, *Non-linear in-plane analysis and buckling of pinned-fixed shallow arches subjected to a central concentrated load*, Int. J. Non-Lin. Mech. **47** (2012), 118–131.
22. Y.-L. Pi, M. Bradford, *In-plane analyses of elastic three-pinned steel arches*, J. Struc. Eng. **141** (2015), 06014009, 1–4.
23. R. A. M. Silveira, C. L. Nogueira, P. B. Gonçalves, *A numerical approach for equilibrium and stability analysis of slender arches and rings under contact constraints*, Int. J. Sol. Struc. **50**(1) (2013), 147–159.
24. G. J. Simitses, D. H. Hodges, *Fundamentals of structural stability*, Elsevier, Boston, 2006.
25. S. t. Yan, X. Shen, Z. Chen, Z. Jin, *On buckling of non-uniform shallow arch under a central concentrated load*, Int. J. Mech. Sci. **133** (2017), 330–343.

26. S. t. Yan, X. Shen, Z. Chen, Z. Jin, *Collapse behavior of non-uniform shallow arch under a concentrated load for fixed and pinned boundary conditions*, Int. J. Mech. Sci. **137** (2018), 46–67.
27. S. t. Yan, X. Shen, Z. Jin, *Instability of imperfect non-uniform shallow arch under uniform radial pressure for pinned and fixed boundary conditions*, Thin-Walled Struc. **132** (2018), 217–236.
28. G. C. Tsiatas, N. G. Babouskos, *Linear and geometrically nonlinear analysis of non-uniform shallow arches under a central concentrated force*, Int. J. Non-Lin. Mech. **92** (2017), 92–101.
29. C. X. Wang, P. Schiavone, *Torsion of elliptical composite bars containing neutral coated cavities*, Theor. Appl. Mech. **43**(1) (2016), 33–47.
30. Y. Zhou, W. Chang, I. Stanciulescu, *Non-linear stability and remote unconnected equilibria of shallow arches with asymmetric geometric imperfections*, Int. J. Non-Lin. Mech. **77** (2015), 1–11.

СТАБИЛНОСТ ПРОСТО-ОГРАНИЧЕНО ОБРТНО ОСЛОЊЕНИХ ЛУЧНИХ НОСАЧА

Резиме. Овај рад има за циљ одређивање критичне силе извијања плитких лучних носача, који имају један крај просто ослоњен док је други крај везан за еластичну ротациону опругу, а у функцији крутости ротационе опруге, геометрије и дистрибуције материјала. Оптерећење је дато у виду концентрисане вертикалне силе која дејствује на врху носача. Дат је геометријски нелинеарни модел који повезује не само аксијалну силу већ и момент савијања са деформацијама мембране. Успостављена је нелинеарна веза између деформације и параметара оптерећења. Ова једначина је потом решена аналитички. Показано је да крутост еластичног ослонца има значајан утицај на најнижу вредност критичне силе извијања. У исто време показује се да нема значајног утицаја овог параметра на геометрију. За нулту вредност крутости ротационе опруге лучни носач постаје обострано просто ослоњен док за случај када вредност крутости тежи бесконачности носач се понаша као да је на једном крају просто ослоњен а на другом уклештен и има најбољу носивост.

Institute of Applied Mechanics
University of Miskolc
Miskolc-Egyetemváros
Hungary
mechkiss@uni-miskolc.hu

(Received 02.04.2020.)
(Available online 02.09.2020.)